

AD 785 543

A

43

RIA-80-U802

USADACS Technical Library



5 0712 01013425 1

**TECHNICAL
LIBRARY**

COPY NO. 1

TECHNICAL REPORT 4711

**PHOTO AND ELECTRIC FIELD EFFECTS
IN ENERGETIC MATERIALS**



D. W. DOWNS	T. GORA
W. GARRETT	M. BLAIS
D. A. WIEGAND	A. C. FORSYTH
H. D. FAIR, JR.	

SEPTEMBER 1974

APPROVED FOR PUBLIC RELEASE; DISTRIBUTION UNLIMITED

**PICATINNY ARSENAL
DOVER, NEW JERSEY**

The findings in this report are not to be construed as an official Department of the Army Position.

DISPOSITION

Destroy this report when no longer needed. Do not return it to the originator.

UNCLASSIFIED

SECURITY CLASSIFICATION OF THIS PAGE (When Data Entered)

REPORT DOCUMENTATION PAGE		READ INSTRUCTIONS BEFORE COMPLETING FORM
1. REPORT NUMBER Technical Report 4711	2. GOVT ACCESSION NO.	3. RECIPIENT'S CATALOG NUMBER
4. TITLE (and Subtitle) PHOTO- AND ELECTRIC FIELD EFFECTS IN ENERGETIC MATERIALS		5. TYPE OF REPORT & PERIOD COVERED
		6. PERFORMING ORG. REPORT NUMBER
7. AUTHOR(s) D.S. Downs, W. Garrett, D.A. Wiegand, T. Gora, M. Blais, A.C. Forsyth, H.D. Fair, Jr.		8. CONTRACT OR GRANT NUMBER(s)
9. PERFORMING ORGANIZATION NAME AND ADDRESS Feltman Research Laboratory Picatinny Arsenal, Dover, New Jersey		10. PROGRAM ELEMENT, PROJECT, TASK AREA & WORK UNIT NUMBERS
11. CONTROLLING OFFICE NAME AND ADDRESS		12. REPORT DATE August 1974
		13. NUMBER OF PAGES 43
14. MONITORING AGENCY NAME & ADDRESS (if different from Controlling Office)		15. SECURITY CLASS. (of this report) UNCLASSIFIED
		15a. DECLASSIFICATION/DOWNGRADING SCHEDULE
16. DISTRIBUTION STATEMENT (of this Report) Approved for public release; distribution unlimited.		
17. DISTRIBUTION STATEMENT (of the abstract entered in Block 20, if different from Report)		
18. SUPPLEMENTARY NOTES		
19. KEY WORDS (Continue on reverse side if necessary and identify by block number)		
Initiation	Ignition	Detonation
Decomposition	Optical absorption	Electronic structure
Lead azide	Photoconductivity	Electronic properties
Colloids	Photodecomposition	Electric field effects
20. ABSTRACT (Continue on reverse side if necessary and identify by block number) The relationship between the pseudostability of explosives and their electronic structure was identified and discussed at the 1972 Army Science Conference. Specifically, direct, non-thermal, photoelectric initiation of certain energetic materials was shown to occur upon simultaneous application of an electric field and light of an appropriate wavelength. To further characterize the microscopic processes responsible for photoelectronic initiation, it is necessary to study in detail the photodecomposition produced by light with no electric field, and to study the initiation by electric fields in the absence of light with particular emphasis on electrode effects.		

DD FORM 1473
1 JAN 73

EDITION OF 1 NOV 65 IS OBSOLETE

UNCLASSIFIED

SECURITY CLASSIFICATION OF THIS PAGE (When Data Entered)

20. Abstract (Continued)

We report here new experimental results which elucidate the mechanism of photoelectronic initiation in lead azide. The spectral and intensity dependence of photodecomposition was monitored by observing the release of nitrogen gas from the azide sub-lattice. Decomposition of the lead sub-lattice was observed by the change in optical density due to formation of colloidal lead. Threshold electric fields have been established for selected metal contacts. A model of the photoelectronic process in lead azide is proposed which takes into account new results from studies of photodecomposition and electric field effects and previous work on photoconductivity and optical absorption. This model predicts that the major effect of light in photoelectronic initiation is to produce a new electric field distribution which leads to detonation.

ABSTRACT

The relationship between the pseudostability of explosives and their electronic structure was identified and discussed at the 1972 Army Science Conference. Specifically, direct, non-thermal, photoelectronic initiation of certain energetic materials was shown to occur upon simultaneous application of an electric field and light of an appropriate wavelength. To further characterize the microscopic processes responsible for photoelectronic initiation, it is necessary to study in detail the photodecomposition produced by light with no electric field, and to study the initiation by electric fields in the absence of light with particular emphasis on electrode effects.

We report here new experimental results which elucidate the mechanism of photoelectronic initiation in lead azide. The spectral and intensity dependence of photodecomposition was monitored by observing the release of nitrogen gas from the azide sub-lattice. Decomposition of the lead sub-lattice was observed by the change in optical density due to formation of colloidal lead. Threshold electric fields have been established for selected metal contacts. A model of the photoelectronic process in lead azide is proposed which takes into account new results from studies of photodecomposition and electric field effects and previous work on photoconductivity and optical absorption. This model predicts that the major effect of light in photoelectronic initiation is to produce a new electric field distribution which leads to detonation.

TABLE OF CONTENTS

	<u>Page No.</u>
ABSTRACT	i
INTRODUCTION	1
BACKGROUND	3
A. Theoretical	3
B. Electronic Structure of Lead Azide	4
C. Previous Photodecomposition and Field Initiation Results	5
EXPERIMENTAL TECHNIQUES & RESULTS	7
A. Crystal Growing	7
B. Photo Effects	9
C. Electric Field Effect and Initiation Studies	11
MODEL FOR THE PHOTOELECTRONIC INITIATION EFFECT	16
CONCLUSIONS	18
ACKNOWLEDGEMENTS	19

	<u>Page No.</u>
Table 1	20

LIST OF FIGURES

Figure 1. Reaction coordinate diagram depicting possible changes in activation energy due to excited electronic states.	21
Figure 2. Comparison of optical absorption spectra of thin film and crystal.	22
Figure 3. Crystal growing apparatus.	23
Figure 4. Solution grown lead azide crystals.	24
Figure 5. Change in optical density due to ultraviolet exposure and calculated optical density (Mie theory) versus wavelength.	25
Figure 6. Photodecomposition spectral response compared to optical absorption.	26
Figure 7. Typical current response to step voltage versus time.	27
Figure 8. Current-voltage characteristic for .025 cm thick lead azide crystal with gold electrodes.	28
Figure 9. Current-voltage characteristic for .073 cm thick lead azide crystal with gold electrodes.	29
Figure 10. Voltage and charge profiles for the constant-field case.	30
Figure 11. Voltage and field profiles resulting from a non-uniform charge distribution E_{ave} = applied voltage/L.	31

INTRODUCTION

At the 1972 Army Science Conference, Fair et al. (1) indicated the possibility that electronic processes in explosive solids could be used to achieve the direct, non-thermal initiation of both primary and secondary explosives. The theoretical basis for the relationship between chemical instability and electronic structure was reviewed, and it was experimentally demonstrated that a number of azide compounds could be initiated by purely electronic means. A combination of a low intensity static electric field and optical excitation in particular spectral regions was found to result in initiation (the photoelectronic initiation or PEI effect). Neither stimulus alone (at the intensities used) produces initiation, and it was shown that the effect could not be explained by purely thermal processes.

A detailed understanding of the microscopic processes involved in the PEI effect in azide compounds would be an important step toward the ultimate goal of achieving the electronic initiation of secondary explosives. Yet this is a monumental undertaking, for two important complications must be overcome: The first involves the nature of the experiments necessary. A large number of parameters must be examined, and their effects characterized; but each data

point consumes at least one single crystal sample. The growth and preparation of these samples is difficult, time-consuming and hazardous. Secondly, the phenomenon being examined is very complex. It involves the simultaneous, time-dependent interaction of effects which can be characterized as electronic (electronic excitation, photoconductivity, perhaps carrier injection and multiplication), chemical (various decomposition processes), and material transport (leading to gas evolution and metal colloid formation), and lead ultimately to a thermal and/or mechanical takeover involving self-sustaining exothermic reactions and detonation.

We report here our recent theoretical and experimental results which lead toward an understanding of the mechanisms involved in the PEI effect in lead azide single crystal samples. Our experimental studies have largely focussed on isolating the effects of optical excitation from those of electric field. Nitrogen gas and metallic lead are the ultimate products of lead azide decomposition. Hence decomposition in the spectral region appropriate to the PEI effect was monitored by directly studying the resulting gas evolution; and changes in the optical absorption were studied as a means of detecting colloidal lead formation. Also reported are electric field and electrode effects on

initiation (without simultaneous optical excitation).

From the results of these investigations we propose a model to account for the PEI effect.

BACKGROUND

A. Theoretical

A general theory relating electronic structure to chemical instability was developed by Williams (2). Briefly, the quantum-mechanical Hamiltonian governing the motion of the nuclei (atoms and/or molecules) in a solid contains an effective potential in terms of internuclear distance \underline{R} .

$$V_{\text{eff}}(\underline{R}) = V(\underline{R}) + E_{e1}(\underline{R})$$

where $V(\underline{R})$ is the interaction potential between nuclei, and $E_{e1}(\underline{R})$ contains the dependence of electronic energies on internuclear separation. As the latter term can vary strongly from one electronic state to another, the internuclear forces governing chemical reactions and therefore decomposition processes can be strongly affected by populating excited electronic states, as shown in Fig. 1.

An explosive solid differs from a reactive gaseous mixture in several important respects. The constituent atoms or molecules are densely packed, leading to their

rather low mobility. Excited electronic states in a solid may differ substantially from the excited states of its constituent atoms or molecules, and in some cases are spatially delocalized over hundreds of atomic or molecular volumes. These states can be excited by optical irradiation of appropriate energy, or by charge injection from appropriate contacts. They may be involved in long-term energy storage. And, perhaps most importantly, the excited electronic states may be mobile in the solid; if they involve charge carriers, external electric fields can influence energy transport, and perhaps lead to avalanching effects.

B. Electronic Structure of Lead Azide

The electronic structure and thermochemistry of azide compounds, and of lead azide in particular, have recently been elucidated (1,3). Lead azide can be viewed as consisting essentially of Pb^{++} and N_3^- ions. The ultimate source of its reactivity is the highly exothermic nature of the conversion of azide ions to nitrogen gas. Thus at some stage, charge transfer is important in the PEI effect as well as in other initiation modes.

Lead azide has an energy band gap of approximately 4eV (3). The highest filled valence band most likely consists of electronic states of N_3^- , and the (unoccupied) conduction band of Pb^+ states. A band gap transition is described as

exciting an electron from an N_3^- state to a Pb^+ state. Lower energy states of excitation are known to exist experimentally (1,3), and have been attributed to either of several types of excitons. While their nature has not been definitively established, the evidence to date appears to favor cationic excitons, consisting of excited states of lead ions $(Pb^{++})^*$. These general features of the electronic structure are, of course, responsible for the manner in which lead azide absorbs light. Figure 2 shows the absorption spectrum of a lead azide thin film sample, as well as the absorption edge for a single crystal sample (3,4).

C. Previous Photodecomposition and Field Initiation Results

Lead azide is known to decompose on exposure to ultraviolet light, giving off nitrogen gas and leaving ultimately a residue of metallic lead or mixtures of lead salts (such as lead oxides and carbonates). With moderate irradiation intensities the decomposition proceeds slowly. With extremely high intensities lead azide detonates and the reaction is completed in a matter of nanoseconds.

All previous photodecomposition studies have been performed on powder and thin film samples, using mainly 253.7nm irradiation. However, the absorption spectrum of lead azide commences at much longer wavelengths in the region of 400nm (refer to Fig. 2). Further, the use of powder and thin film

samples has made the data difficult to interpret, and often not reproducible because of the contributions of surface, interface, particle size and defects associated with powders and films. Hence to understand these phenomena it was necessary to examine the spectral response and intensity dependence of photodecomposition efficiency for single crystal samples of lead azide.

No previous attempts have been made to examine what happens to lead ions during photodecomposition. For reasons of overall charge neutrality, either neutral lead or lead salts are expected to form. A study of changes in the absorption spectrum as a function of prior irradiation and history was hence undertaken in an attempt to observe colloidal lead particles, again using single crystal samples.

Finally, a number of field initiation studies have been reported (5) for lead azide. All such studies to date have been performed on pressed pellet and powder samples and the results have therefore varied with particle size distribution and overall density. A number have involved at least one electrode not in contact with the sample; thus air breakdown corona discharges were important in their interpretation. Studies to date have yielded little information on electric field effects in the bulk of a lead azide sample. To gain an understanding of these complex phenomena it was necessary

to determine the condition under which electric fields induce initiation of single crystals of lead azide for a particular electrode material and sample-electrode geometry. Our configuration and contact choices were made to maximize the chances for current injection and minimize surface effects.

EXPERIMENTAL TECHNIQUES & RESULTS

A. Crystal Growing

The most critical obstacle to the experimental study and understanding of electronic initiation has been the lack of single crystals of sufficient size, purity and optical quality. Previous efforts to grow lead azide crystals gave rather discouraging results, with detonations of the crystal-growing solutions resulting in the loss of crystals and of equipment as well. Thus the task of developing a safe reliable method of crystal growth was undertaken using recent developments in the solution chemistry of azides, along with modifications of the techniques of crystal growth from solutions used for other compounds.

The lead azide crystal growing apparatus (6) is shown in Fig. 3. To limit the amount of explosive material in any one container and to ensure against the loss of hydrazoic acid at high temperatures, pyrex test tubes with screw caps

containing silicone rubber gaskets were used as the growing vessels. The aluminum block used to hold the test tubes inside the polycarbonate container also served to isolate the test tubes from each other should explosions occur. A proportional temperature controller with a platinum sensor and a 200 watt immersion heater maintained temperature control to within 0.01°C . The crystals were grown by slowly cooling saturated ammonium acetate solutions from 70°C at a rate of $0.5^{\circ}\text{C}/\text{day}$.

Harvesting the crystals is a critical step. Spontaneous explosions occur if all the crystal-growing solution is not immediately washed from the crystal surfaces. The best procedure involves pouring the solution and crystals from the test tube onto a porous cloth covering a ceric ammonium nitrate solution and immediately rinsing with warm distilled water. The azide remaining in solution is thus destroyed in the ceric solution.

X-ray precession photographs show that the resulting optically clear crystals are orthorhombic, the alpha-form of lead azide. The diffraction spots are sharp and there is no evidence of twinning. The largest crystals have approximate dimensions of $1.0 \times 0.5 \times 0.5$ cm. No attempt was made to grow larger samples because of the danger involved in handling them. However, for most of the

optical and electronic measurements, techniques had to be developed to cut and polish the crystals. The as-grown crystals normally develop one or more large faces that can be conveniently glued to a holding rod (with beeswax). Plates can then be cut with reference to the natural face. The cutting is accomplished with a string saw using a dilute ceric ammonium nitrate solution as the chemical cutting agent. The resulting crystal plates are then polished on a slow speed polisher using a micro-polishing cloth and a polishing compound of medium to very fine grain size. Figure 4 shows typical plates cut from large crystals as well as two uncut crystals in the bottom row.

B. Photo-Effects

To understand the detailed nature of the effects of irradiation on lead azide, optical transmission and mass spectrometric techniques were utilized. The optical transmission measurements were performed on cut and polished lead azide single crystal plates mounted in a vacuum cryostat (pressures of 10^{-3} to 10^{-5} Torr) in a Cary 14 R spectrophotometer. The optical density or fraction of light absorbed in passing through the sample was measured as a function of wavelength or energy and was determined at sample temperatures of 12, 78 and 300K. Changes in the optical density were measured following irradiation of the

lead azide sample with a high pressure mercury lamp (250 watts) and appropriate filters.

The evolution of gas from single crystals was measured in a Varian ultra-high vacuum system utilizing a Vac-Ion pump to achieve base pressures of 10^{-8} Torr. The samples were irradiated with monochromatic light from a 1000 watt Mercury-Xenon lamp through a quartz prism monochromator. The gas was detected either with a residual gas analyzer mass spectrometer or a Bayard-Alpert type vacuum gage. With this technique a monolayer of decomposition from the surface of a single crystal could be detected.

The optical transmission studies (7) indicate that the change in optical density produced in lead azide exposed to blue and ultraviolet irradiation results in the formation of colloids of metallic lead. In Fig. 5, the experimentally observed increase in optical density (due to irradiation of a lead azide single crystal with ultraviolet light) is given as a function of wavelength. The calculated optical density of a lead azide sample containing spherical (up to about 10nm diameter) lead colloids, using the Mie Theory, is also shown in Fig. 5. The good agreement between the observed and calculated optical spectra, plus the lack of temperature dependence of the optical density in irradiated crystals, indicate that ultraviolet and blue light irradiation of lead azide single crystals produce lead colloids.

The efficiency (number of N_2 molecules evolved/incident photon/sec) of the evolution of nitrogen gas from a large single crystal plate of lead azide has been studied as a function of wavelength of the exciting light, and the results, together with the optical absorption of lead azide, are shown in Fig. 6. The kinetics and energetics of the reactions and the specific electronic processes and transitions giving rise to the decomposition have been discussed elsewhere (8). The major result for this work concerns the magnitude of the quantum efficiency for the evolution of nitrogen gas (less than 10^{-5}) near the onset of optical absorption. The spectral dependence of the efficiency closely follows the optical absorption.

C. Electric Field Effect and Initiation Studies

To gain an understanding of the effect of the electric field in the absence of photo-effects a detailed study of the current-voltage characteristics and thickness dependence was made. Gold electrodes were applied to both sides of single crystal lead azide plates by vacuum evaporation. These gold electrodes were then contacted by gold wires using dots of silver paint. Sample thickness varied from .019 to .076 cm in this series of experiments. The electrode diameter, 2.36mm, was the same on all samples.

By keeping the evaporated electrode diameter large compared to the sample thickness, the results can be analyzed on the basis of one-dimensional planar current flow (9). An advantage of the sandwich-type electrode configuration is that surface currents can then be essentially eliminated. The samples were potted in RTV, a polymeric electronic potting composition, which aids in prohibiting current flow by any path other than through the bulk of the sample.

The sample chamber was evacuated by a forepump with an in-line liquid nitrogen trap. With samples of the size used in these experiments, the chamber is not damaged by the detonation. Performing the experiments under this type of vacuum is sufficient to eliminate the shock wave resulting from sample detonation and any dependence of the results on atmospheric humidity conditions.

An inherent procedural difficulty arose because of the possibility that lead azide crystals subjected to high electric fields may experience localized decomposition or other damage prior to detonation. This could act as a memory of previous treatment and might influence both the conductivity and critical voltage for detonation. One solution would be to use a fresh crystal for each value of applied voltage. However, this procedure would require an unrealistic number of samples with accurately controlled

thickness. To minimize memory effects, each sample was subjected to the same voltage history. Our procedure consists of one-minute-on one-minute-off application of voltage, increasing the voltage in 100V increments. The procedure was continued until the sample detonated, with current being monitored continuously. A typical current-response is shown in Fig. 7.

The current has a negative transient when the voltage is turned off which is not shown. Seven samples of varying thickness were investigated in this manner. The voltage at which detonation occurred, (V_{DET}), is shown in Table I along with the current just prior to initiation, I . It should be noted that the detonation does not necessarily occur immediately upon application of the voltage. The delay time was observed to vary. Typical current-voltage characteristics are shown in Figs. 8 and 9 and reflect the non-ohmic nature of the Au/lead azide system.

In a very simplified picture the voltage applied to the crystal can under some circumstances produce a constant average electric field in the sample given by V/L , where L is the sample thickness. It is assumed here that the contacts to the crystal do not affect the field distribution in any way, that is, the contacts are ohmic. On the other hand, it is possible that the contacts to the sample are

non-ohmic and restrict the flow of current. This kind of contact is called a blocking or rectifying contact; and, because it can present more resistance to current flow than the bulk resistance of the sample, the field distribution may be altered considerably. Gold forms a non-ohmic contact with lead azide (10). The effectively higher resistance of the Au/lead azide interface can result in a significant voltage drop across this region, with considerably less voltage actually applied across the bulk of the sample.

The average fields for detonation, calculated for each crystal from V_{DET} divided by the sample thickness L , range from 3.02×10^4 - 4.21×10^4 V/cm. Thus there is a threshold in this field range at which detonation occurs. The scatter in values could be accounted for by differences in the crystal-electrode interfaces or differences due to crystal orientation. The threshold field values for the four thinnest samples (.019 - .025 cm) are all higher than those for the thicker samples (.043 - .076 cm). This would be expected if effects resulting from exposure to electric fields tend to lower the field threshold since the thicker samples experienced longer cumulative exposure times to electric fields.

MODEL FOR THE PHOTOELECTRONIC INITIATION EFFECT

The photolytic and electric field studies have led to a number of specific and general conclusions on the individual phenomena investigated. Our purpose, however, was not only to understand the separate phenomena but to relate them to understand the nature of the more complex PEI effect. It is now possible to infer a mechanism for the PEI effect.

We first review the evidence pertinent to the mechanism. Neither the field alone nor the light alone, at the intensities used, can produce initiation by simple thermal effects (1). Similarly, the combination of light and electric field intensities used in the PEI effect are not sufficient to lead to initiation thermally (1,11). Even if all of the energy released by exothermic photodecomposition reactions is taken into account, the magnitude of the efficiency for photodecomposition is far too small to provide sufficient thermal energy to initiate fast decomposition. The exciting light does lead to the production of nitrogen gas and to the formation of lead colloids. The resulting decomposition may produce energy states which enhance reaction. In addition, the exciting light produces large changes in the electrical conductivity (up to four orders of magnitude) by the production of

photocarriers (1). Initiation clearly occurs in response to an applied electric field, and an average field value has been determined experimentally.

In order to initiate lead azide by light alone, an intensity six orders of magnitude greater than that used in our experiments is required (1). However, with the low light intensity used in the PEI effect, the value of the applied voltage is of the order of half that required to initiate with electric field alone. Therefore the primary effect of the exciting light combined with the applied electric field is to change the electric field distribution in the lead azide. This accounts for the factor of two or more decrease in average electric field necessary to achieve initiation with light. Figure 10 depicts a uniform voltage drop, which by Maxwell's equations predicts a constant electric field and overall zero net charge. This approximates conditions in the bulk of the crystal in the absence of light, and is generally correct independent of the nature of the contact/sample interface. When the light is turned on, charge carriers of both signs are produced, either directly or through the intermediate step of exciton formation. The original applied electric field separates charge carriers of opposite sign. The resulting charge distribution alters the electric field

distribution. The nature and degree of the charge separation are related to the carriers' conductivity properties, the intrinsic defect structure of the crystal, and possibly to the photo-produced defects. Colloidal particles can act as sources or traps for charge carriers, and will be present near the illuminated surface. In addition, the charge distribution can be strongly affected by the presence of blocking contacts which prohibit the flow of charge into and out of the sample. Charge can accumulate at the interface, producing high fields across the contact region, and considerably altering the field in the bulk. For example, the arbitrarily chosen charge distribution shown in Fig. 11 leads to the indicated voltage and field distributions. The important point is that upon illumination, the resulting photo-induced charge distribution leads to an increase in the electric field at some point in the sample by a factor of two or more above that which it had in the nonilluminated case. This increase in internal electric field is sufficient to produce initiation.

Although there is not yet a clear understanding of why a threshold electric field at a given region of the sample causes initiation, one plausible explanation is that the electric field produces an avalanching multiplication of charge carriers. This results in a region of dense

electronic excitation leading to an ultimate exothermic process. This is further supported by the fact that low-intensity light alone does not produce these regions of dense electronic excitation.

CONCLUSIONS

Our theoretical studies (1) indicated the possibility of initiating decomposition and detonation by several radically new mechanisms. The photoelectronic initiation effect in lead azide was the first experimental observation of the initiation of detonation by purely non-thermal electronic processes. To understand this phenomenon, techniques were developed to grow, cut and polish large pure single crystals of lead azide. The separate effects of light and electric fields on lead azide single crystals were studied to determine the detailed mechanisms of the interactions. These were related to develop an understanding of the PEI effect in terms of threshold average electric fields. Illumination creates photocarriers which change the electronic charge distribution within the lead azide, raising the electric field to the threshold for initiation. These results provide the understanding to apply the photoelectronic initiation effect to other technologically important explosives, and provide the rational basis for pursuing related mechanisms for initiation.

ACKNOWLEDGEMENTS

We are grateful for helpful discussions with
Professors Peter Mark and F.E. Williams.

TABLE I

Electric Field Effects on Lead Azide

<u>Sample</u>	<u>Thickness L (cm)</u>	<u>Current at Detonation (amp)</u>	<u>Voltage at Detonation V_{DET}</u>	<u>Threshold Field V_{DET}/L (Volts/cm)</u>
3-72-30	.019	1.2×10^{-9}	800	4.20×10^4
3-72-31	.024	6.9×10^{-8}	1000	4.17×10^4
3-72-32	.022	7.0×10^{-9}	800	3.60×10^4
3-72-33	.043	1.6×10^{-8}	1300	3.02×10^4
3-72-34	.025	1.4×10^{-8}	1000	4.00×10^4
3-72-35	.076	5.5×10^{-9}	2700	3.54×10^4
3-72-36	.073	1.1×10^{-8}	2400	3.26×10^4

REACTION COORDINATE DIAGRAM

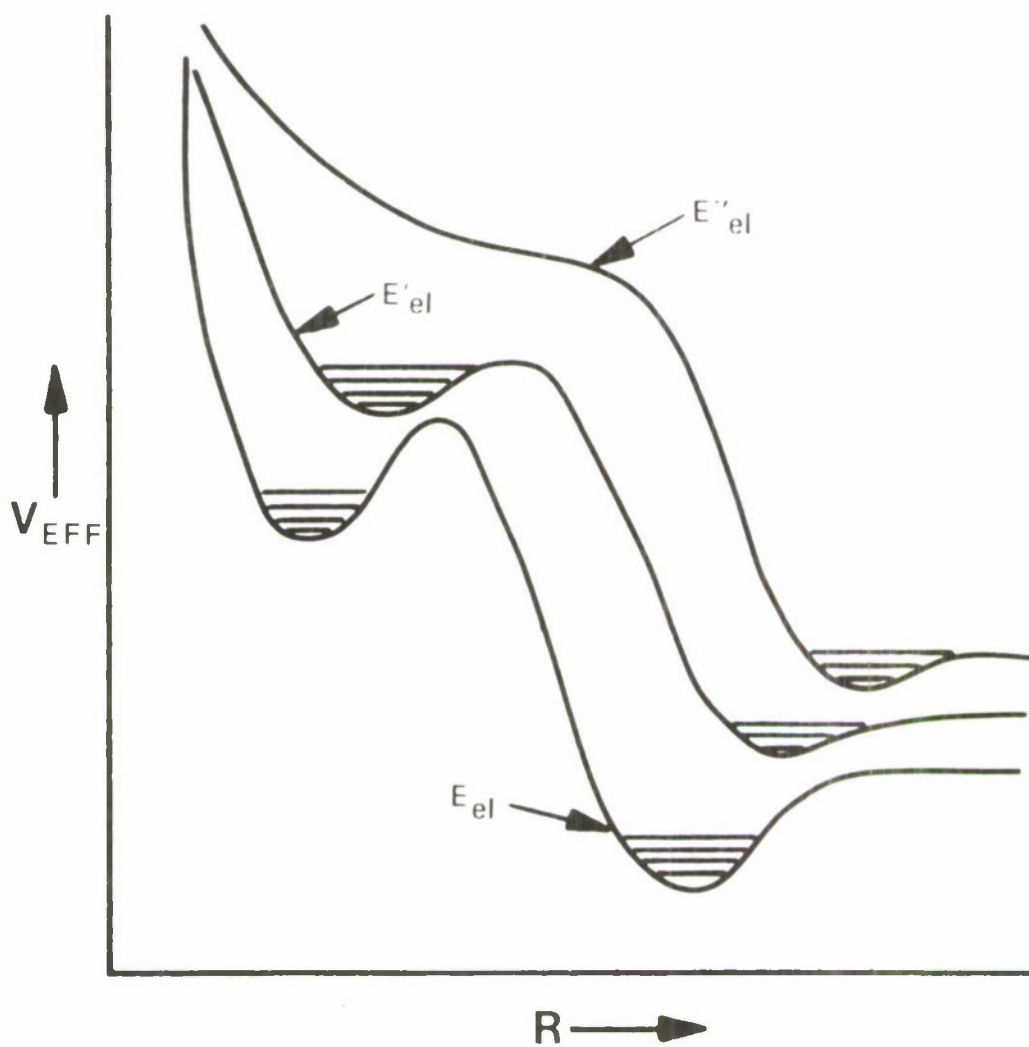


FIGURE 1. Reaction coordinate diagram depicting possible changes in activation energy due to excited electronic states.

OPTICAL ABSORPTION OF LEAD AZIDE CRYSTAL AND THIN FILM

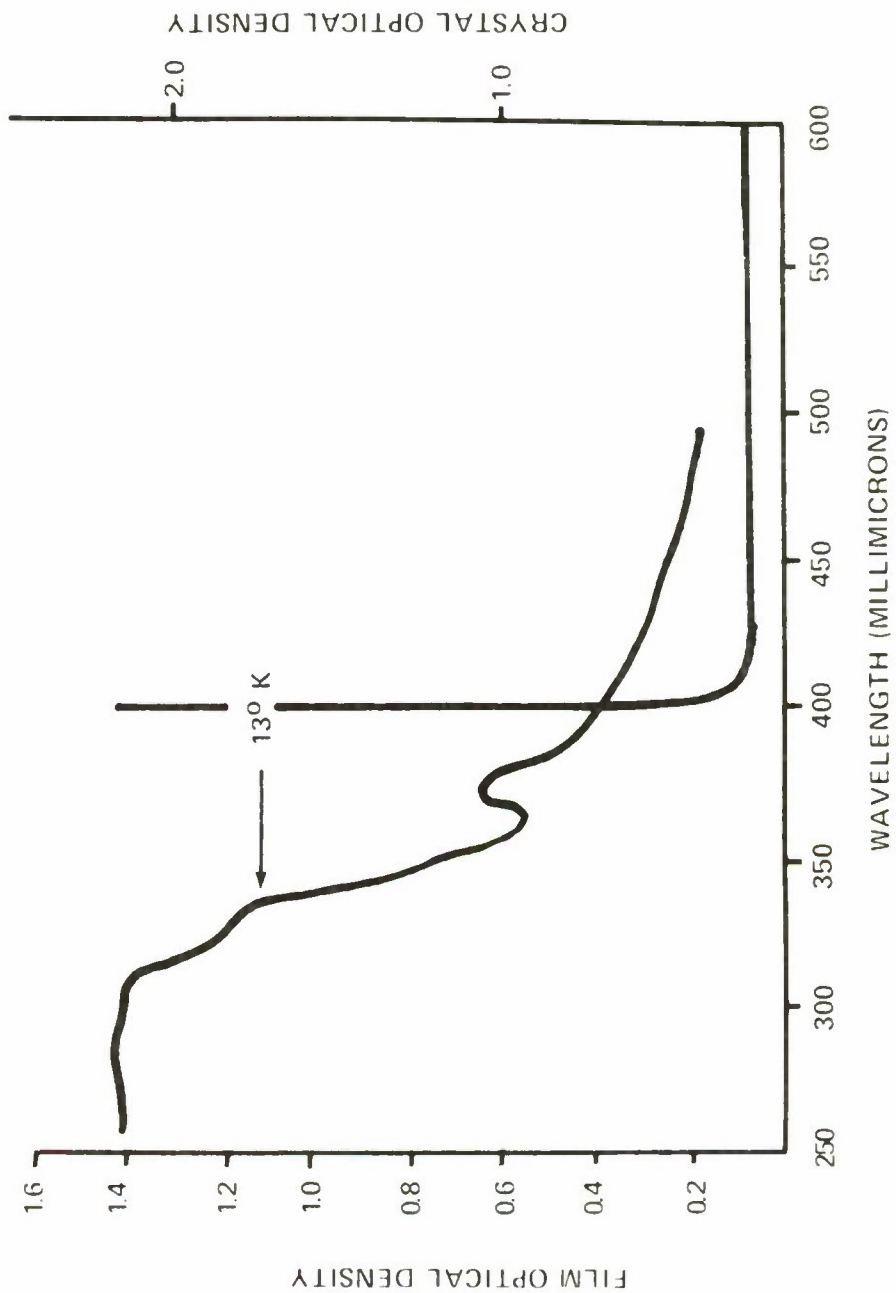


FIGURE 2. Comparison of optical absorption spectra of thin film and crystal.

CRYSTAL GROWING APPARATUS

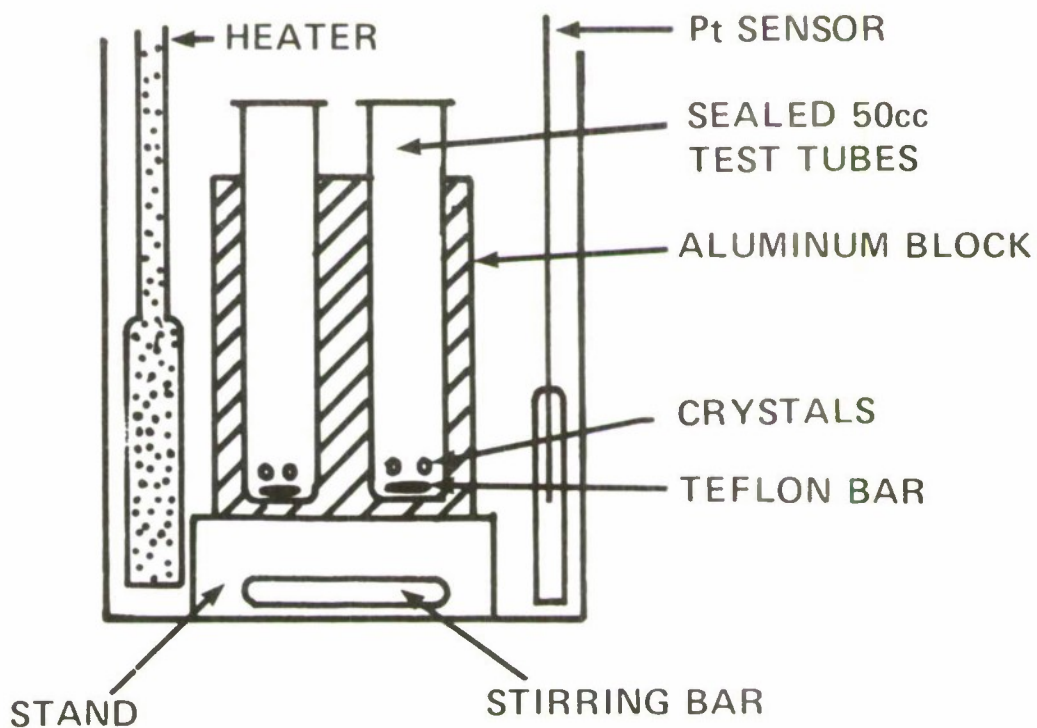


FIGURE 3. Crystal growing apparatus.

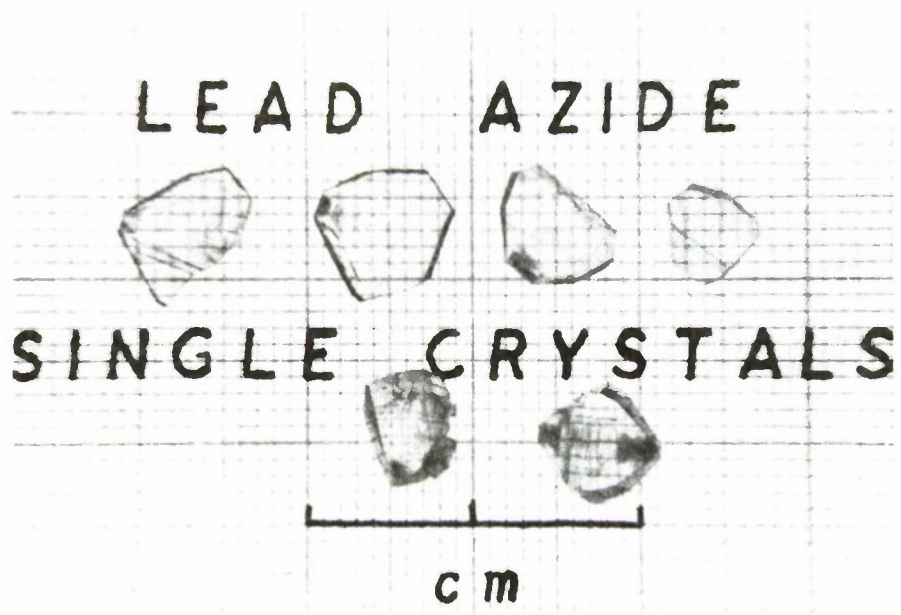


FIGURE 4. Solution grown lead azide crystals.

CHANGE IN OPTICAL DENSITY

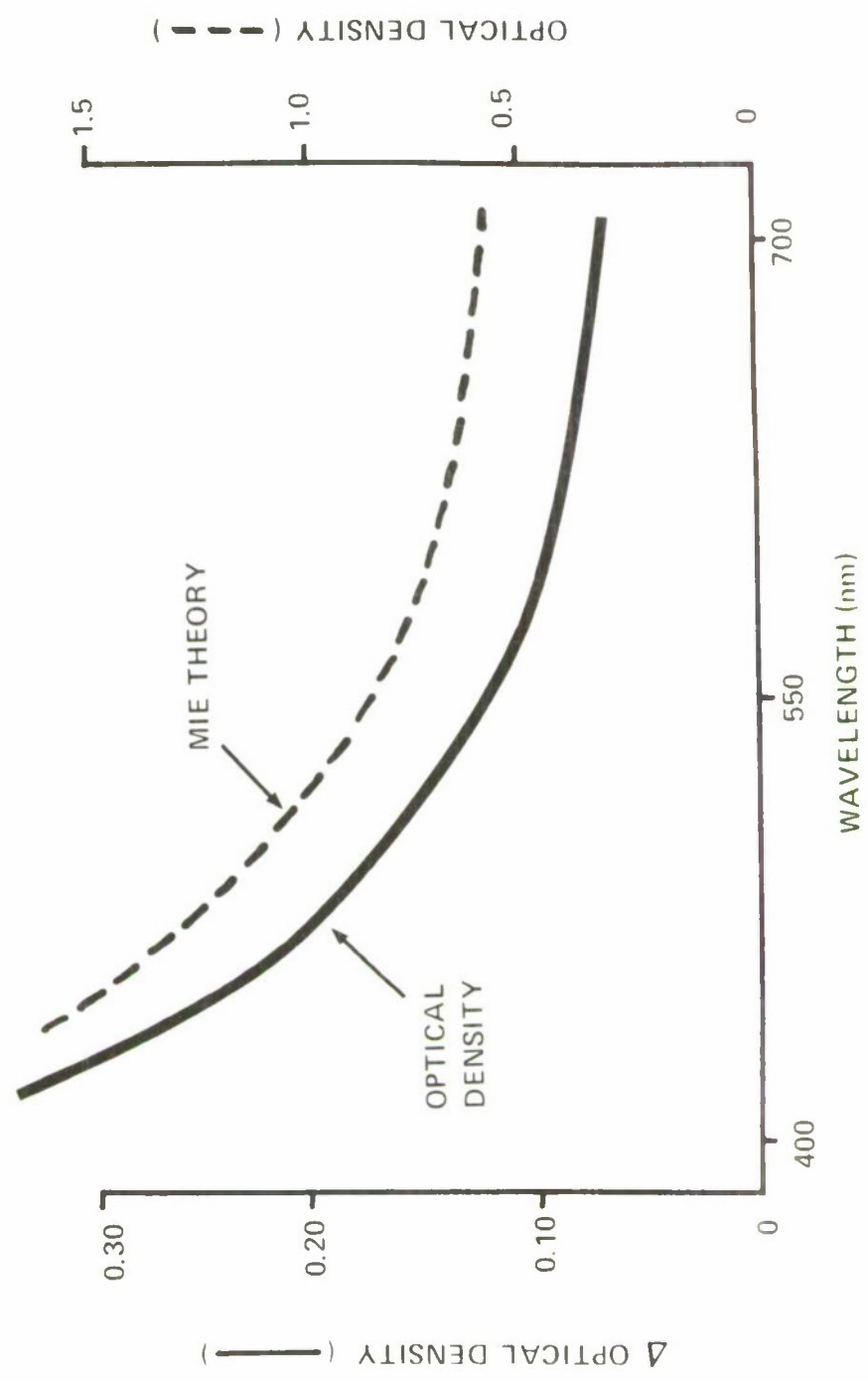


FIGURE 5. Change in optical density due to ultraviolet exposure and calculated optical density (Mie theory) versus wavelength.

PHOTO DECOMPOSITION AND OPTICAL ABSORPTION

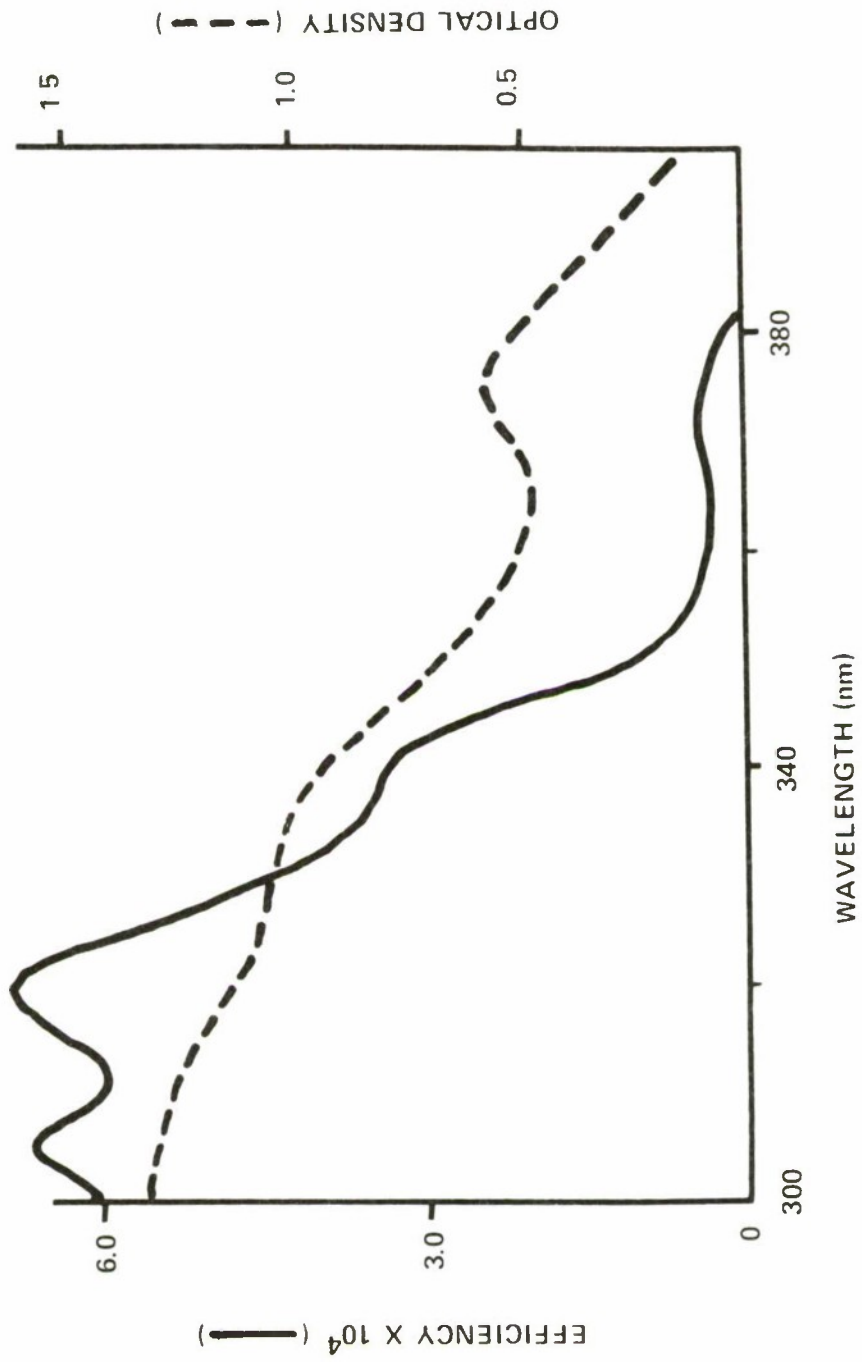


FIGURE 6. Photodecomposition spectral response compared to optical absorption.

CURRENT RESPONSE VS TIME

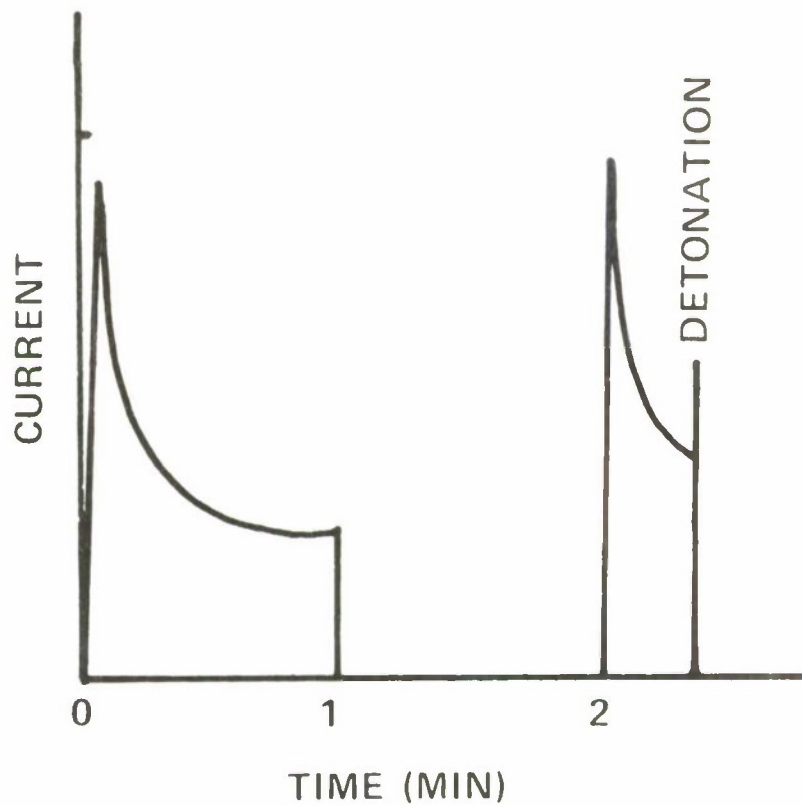


FIGURE 7. Typical current response to step voltage versus time.

CURRENT VOLTAGE CHARACTERISTICS

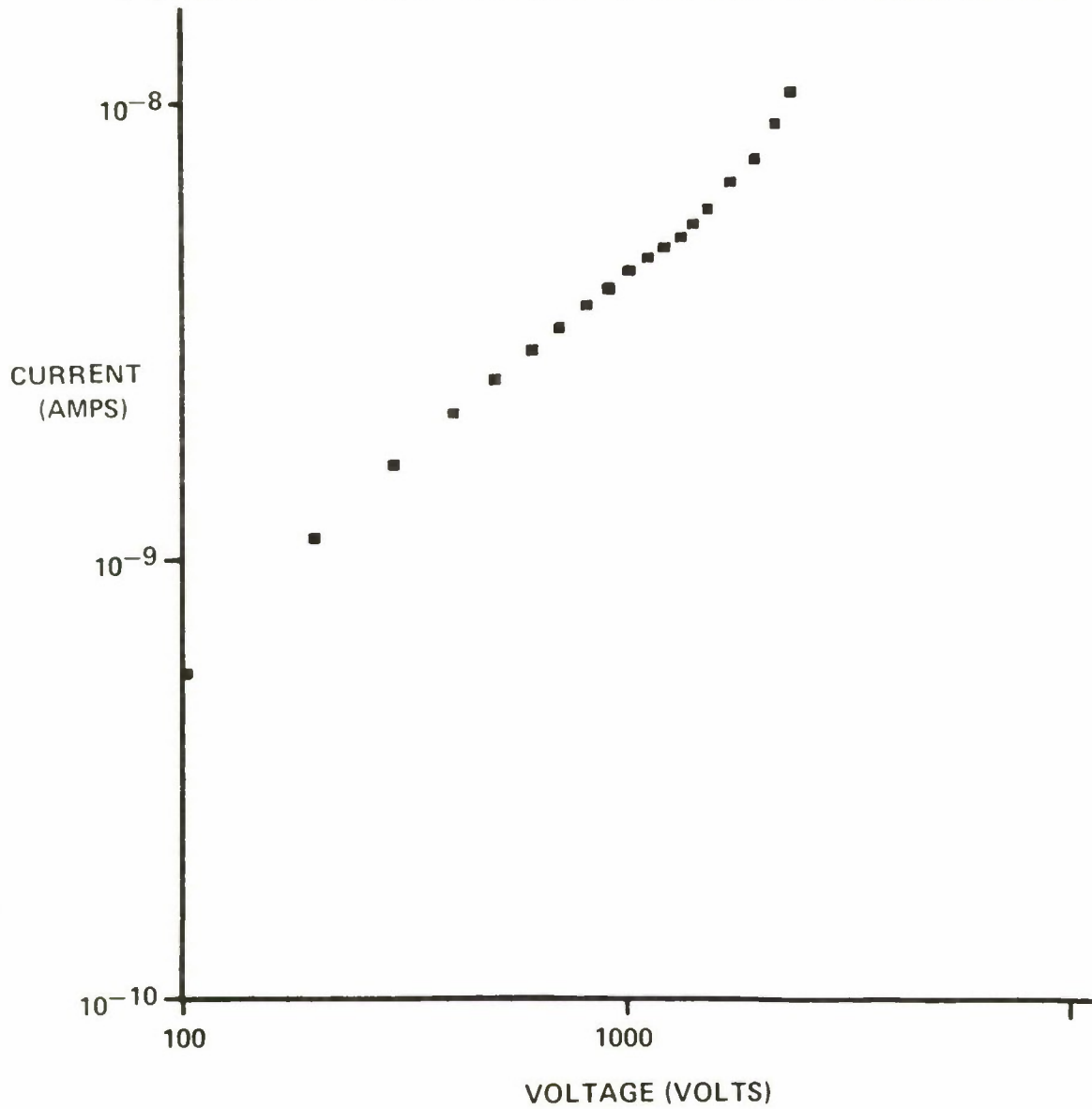


FIGURE 8. Current-voltage characteristic for .025 cm thick lead azide crystal with gold electrodes.

CURRENT VOLTAGE CHARACTERISTICS

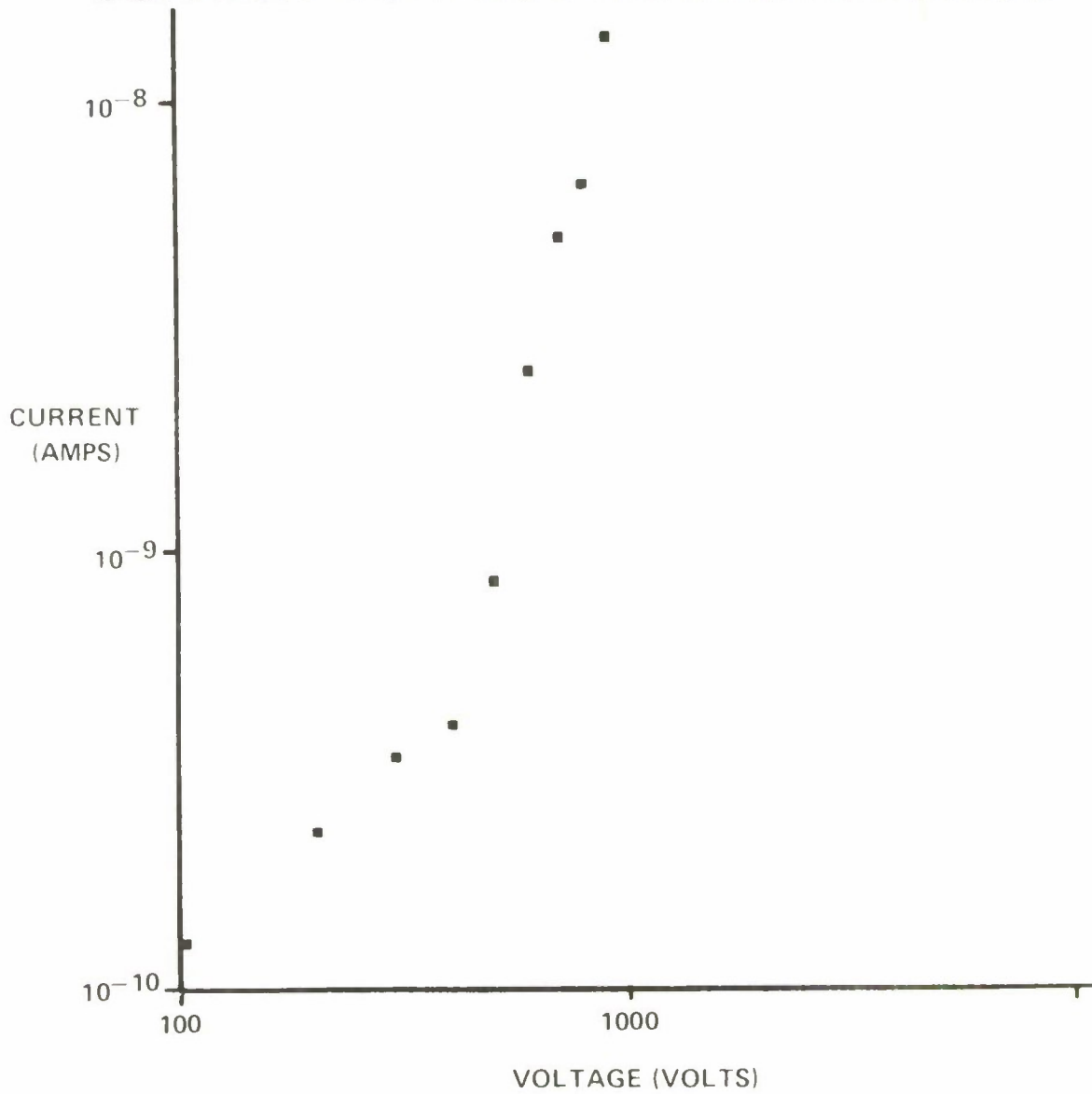


FIGURE 9. Current-voltage characteristic for .073 cm thick lead azide crystal with gold electrodes.

ELECTRIC FIELD DISTRIBUTION

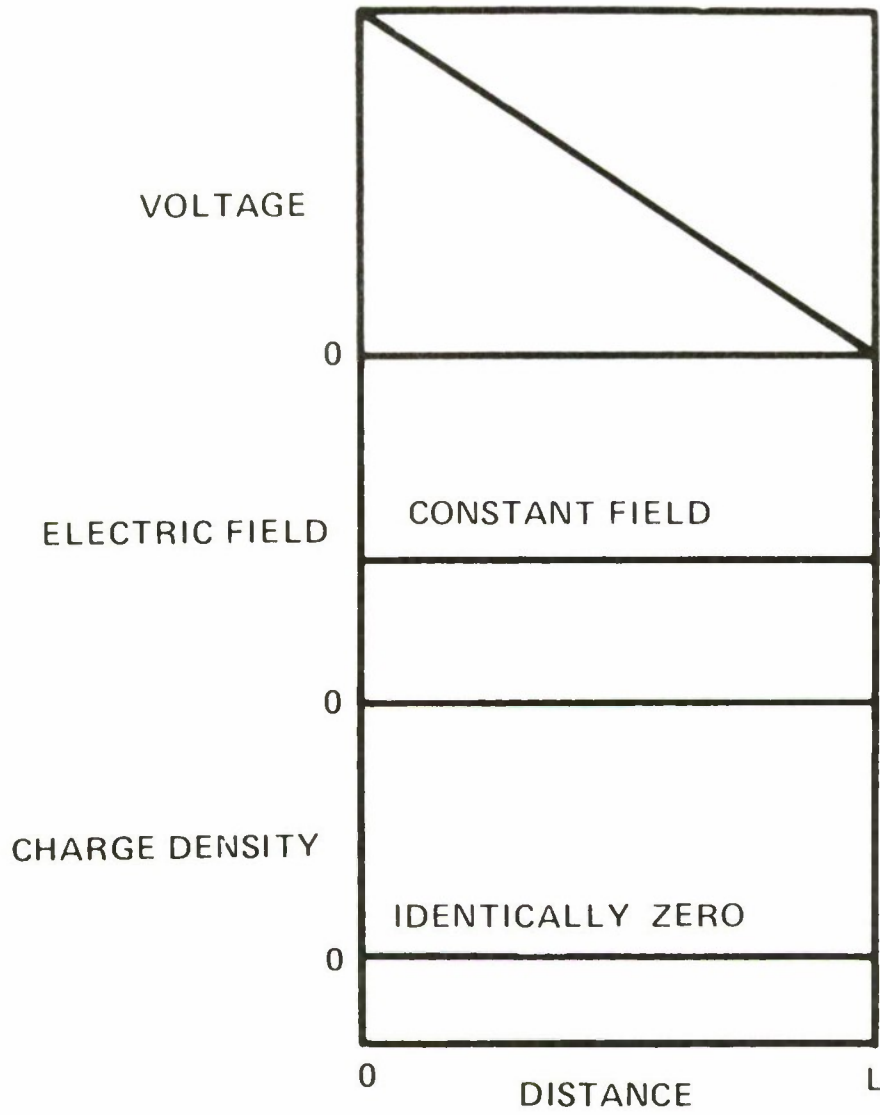


FIGURE 10. Voltage and charge profiles for the constant-field case.

ELECTRIC FIELD DISTRIBUTION

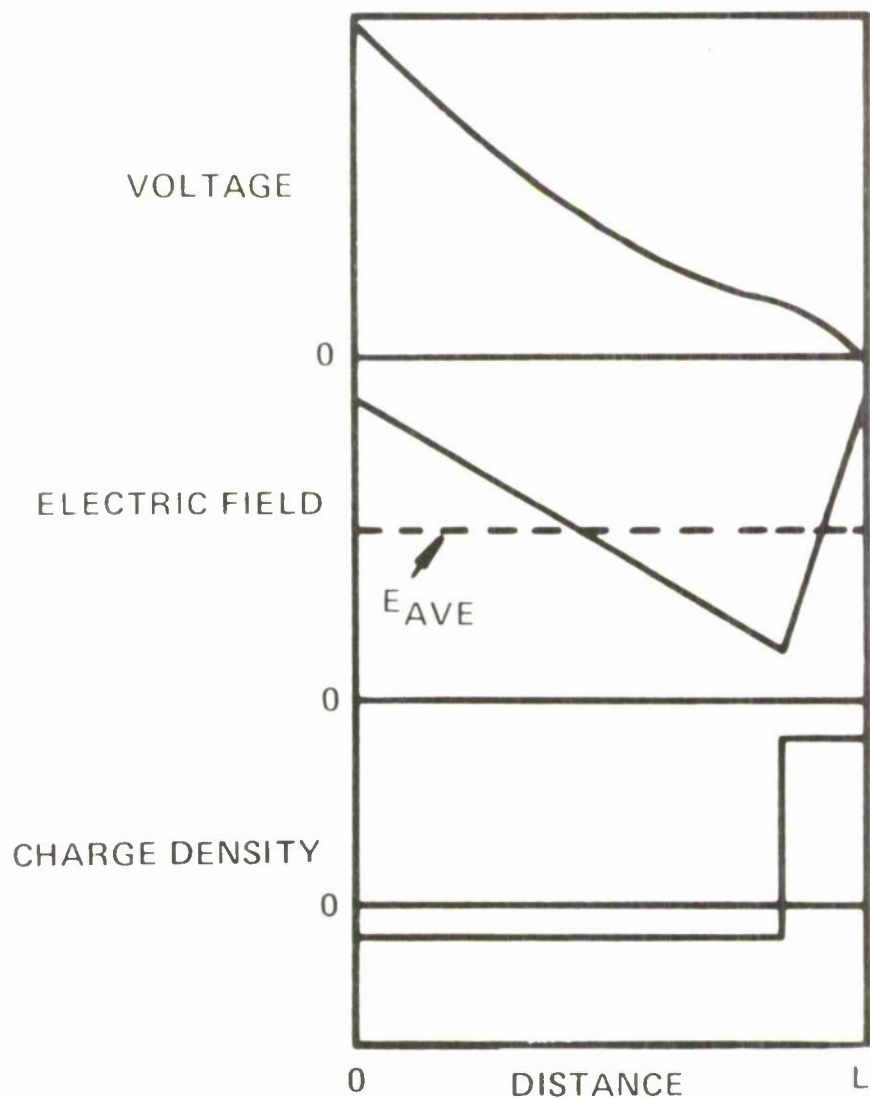


FIGURE 11. Voltage and field profiles resulting from a non-uniform charge distribution $E_{ave} = \text{applied voltage}/L$.

REFERENCES

1. H.D. Fair, D.S. Downs, A.C. Forsyth, M. Blais and T.F. Gora, in Proceedings of Army Science Conference, West Point (1972).
2. F.E. Williams in Chemical Dynamics, J.O. Hirshfelder and D. Henderson, Editors (Wiley-Interscience, New York 1971), p. 289.
3. D.S. Downs and T.F. Gora in High Energy Chemistry: Physics and Chemistry of the Inorganic Azides, H.D. Fair, Editor (Plenum, New York, in publication).
4. H.D. Fair and A.C. Forsyth, J. Phys. Chem. Solids 30, 2559 (1969).
5. See for example, H.S. Leopold, Naval Ordnance Laboratory Tech. Rept. 73-125 (1973) and M.S. Kirshenbaum PATR 4559 (1973).
6. W.L. Garrett, Mat. Res. Bull. 7, 949 (1972).
7. D.A. Wiegand, PATR 4080 (1970).
8. W. Garrett in High Energy Chemistry: Physics and Chemistry of the Inorganic Azides, H.D. Fair, Editor (Plenum, New York, in publication).
9. M. Lampert and P. Mark, Current Injection in Solids (Academic Press, New York 1970).
10. D.S. Downs, PATR (in publication).
11. D.S. Downs, T.F. Gora and M. Blais, PATR (in publication).

DISTRIBUTION LIST

Copy No.

Commander	
Picatinny Arsenal	
ATTN: Mr. H.W. Painter	1
Dr. E.G. Sharkoff	2
Scientific and Technical Information Branch	3-7
Dover, NJ 07801	
Commander	
US Army Materiel Command	
ATTN: AMCDL, Dr. J.V.R. Kaufman (AMCRD)	8
AMCRD, Dr. R.B. Dillaway (AMCDL)	9
Dr. H. El Bisi (AMCRD-T)	10
5001 Eisenhower Avenue	
Alexandria, VA 22333	
Commander	
US Army Armament Command	
ATTN: AMSAR-RD-T	11
AMSAR-SF	12
Rock Island, IL 61201	
Commander	
US Army Ballistic Research Laboratories	
ATTN: Dr. R.J. Eichelberger, Director	13
Dr. I. May	14
Dr. A. Barrows	15
Dr. K. White	16
Dr. E. Freeman	17
Aberdeen Proving Ground	
Maryland 21005	
Commander	
Army Research Office (Durham)	
ATTN: Dr. D.R. Squire	18
Dr. C. Boghosian	19
Dr. R. Ghirardelli	20
Dr. H. Wittmann	21
Box CM, Duke Station	
Durham, NC 28806	

	<u>Copy No.</u>
Commander US Naval Weapons Center (Code 753)	
ATTN: Technical Library	22
Dr. R. Reed	23
Dr. H. Gryting	24
Dr. T. Joyner	25
Mr. J. Pakulak	26
China Lake, CA 93555	
 Dr. John A. Brown	 27-28
P.O. Box 145	
Berkeley Heights, NJ 07922	
 Commander US Naval Ordnance Laboratory	
ATTN: Technical Library	29
Dr. M. Kamlett	30
Mr. I. Kabik	31
Mr. H. Leopold	32
Mr. L.J. Montesi	33
White Oak, Silver Spring Maryland 20910	
 Director US Naval Research Laboratory	
ATTN: Code 2027	34
Washington, DC 20350	
 US Naval Ordnance Station	
ATTN: Library	35
Indian Head, MD 20640	
 Commander Frankford Arsenal Pittman-Dunn Laboratories	
ATTN: Dr. J. Lannon	36
Bridge and Tacony Streets Philadelphia, PA 19137	
 Explosives Research Laboratories Bureau of Mines	
ATTN: Dr. R.W. Watson	37
Dr. R. Van Dolah	38
Pittsburgh, PA 15230	

Copy No.

Headquarters
Air Force Weapons Laboratory (WLX) 39
Kirtland Air Force Base, NM 87117

Commander
Armament Development & Test Center
Eglin AFB
ATTN: Dr. L. Elkins 40
Valpariso, FL 32542

Commander
Harry Diamond Laboratories
ATTN: Technical Library 41
Washington, DC 20438

Los Alamos Scientific Laboratory
ATTN: GMX-2, Dr. L. Smith 42
M-3, Dr. B. G. Craig 43
GMX-2, Dr. H. Cady 44
WX-3, Dr. A. Popolato 45
Technical Library 46
Los Alamos, NM 87544

Lawrence Livermore Laboratory
ATTN: Technical Library 47
Mrs. B. Dobratz 48
Dr. F. Walker 49
PO Box 808
Livermore, CA 94550

Sandia Corporation
ATTN: Dr. A. Strasburg 50
Dr. T. Tucker 51
Dr. J. Gover 52
Dr. N. Brown 53
Technical Library 54
Albuquerque, NM 87115

Air Force Office of Scientific Research 55
1400 Wilson Boulevard
Arlington, VA 22209

Copy No.

Redstone Scientific Information Center US Army Missile Command ATTN: Chief, Document Center Redstone Arsenal, AL 35808	56
Scientific and Technical Information Facility ATTN: NASA Representative (S-AK/DL) PO Box 5700 Bethesda, MD 20014	57
Department of the Army Office, Assistant Chief of Staff Research Branch - R&D Division ATTN: Scientific Information Section Washington, DC 20315	58
Stanford Research Institute Fluid Physics & Detonation Dynamics Dept. ATTN: Dr. R. Shaw Dr. M. Cowperthwaite Menlo Park, CA 94025	59 60
US Atomic Energy Commission ATTN: Division of Technical Information Oak Ridge, TN 37830	61
Mr. Jack R. Polson Mason and Hanger - Silas Mason Co. Development Section, IAAP Burlington, IA 52601	62
Dr. L. A. Rosenthal Department of Electrical Engineering Rutgers University New Brunswick, NJ 08903	63
Dr. J. Kestin Department of Engineering Brown University Providence, RI 02912	64
Dr. S. S. Mitra Department of Electrical Engineering University of Rhode Island Kingston, RI 02881	65

	<u>Copy No.</u>
Dr. B.S.H. Royce Department of Aerospace & Mechanical Sciences Princeton University Princeton, NJ 08540	66
Dr. R. A. Schmitz Engineering Experiment Station University of Illinois Urbana, IL 61803	67
Dr. Vincent Menichelli Jet Propulsion Laboratory 4800 Oak Grove Drive Pasadena, CA 91103	68
Dr. J. C. Yang Jet Propulsion Laboratory 4800 Oak Grove Drive Pasadena, CA 91103	69
Dr. C. R. Westgate Department of Electrical Engineering Johns Hopkins University Baltimore, MD 21218	70
Dr. Peter Mark Department of Electrical Engineering Princeton University Princeton, NJ 08540	71
Dr. Fred P. Stein Department of Chemical Engineering Lehigh University Bethlehem, PA 18015	72
Dr. M. J. Strauss Department of Chemistry University of Vermont Burlington, VT 05401	73
Dr. Martin Summerfield Department of Aerospace & Mechanical Sciences Princeton University Princeton, NJ 08540	74

	<u>Copy No.</u>
Dr. N. Geacintov Department of Physics New York University New York, NY 10053	75
Dr. F. E. Williams Department of Physics University of Delaware Newark, DE 19711	76
Hyman A. Golopol, L-402 Lawrence Livermore Laboratory P.O. Box 808 Livermore, CA 94550	77
Defense Documentation Center Cameron Station Alexandria, VA 22314	78-89
Commander Picatinny Arsenal ATTN: Dr. D.S. Downs SARPA-FR-E-S Dover, NJ 07801	90-99